Int. J. Heat Mass Transfer. Vol. 27, No. 11, pp. 2047–2056, 1984
Printed in Great Britain

0017-9310/84 $3.00 + 0.00
Pergamon Press Ltd.

Convective heat losses from a pipe buried in a semi-infinite porous medium

HAIM H. BAU

Department of Mechanical Engineering and Applied Mechanics,
University of Pennsylvania, Philadelphia, PA 19104, U.S.A.

(*Received* 25 *February* 1983 *and in revised form* 30 *January* 1984)

Abstract—An analytical solution is presented for steady-state low Rayleigh number convection induced by a pipe buried in a saturated, semi-infinite, permeable medium. The medium surface may be inclined with respect to the gravity vector. Both the cylinder and the medium surfaces are maintained at constant uniform temperatures. Two cases are considered. In the first case, the surface of the medium is impermeable to fluid motion while in the other percolation through this surface is allowed. The complicated geometry is handled in an elegant manner through the use of bicylindrical coordinates. The results include a description of the flow and the temperature fields as well as a correlation for the Nusselt number. In addition, it is demonstrated that an optimal burial depth exists for which heat losses from the pipe are minimized. The analytical results are compared with numerical calculations.

1. INTRODUCTION

IN RECENT years, the problem of heat losses from buried pipes has received considerable attention. This problem arises, for example, in connection with oil/gas lines where the oil/gas is heated or chilled in order to reduce pumping power, as well as in the context of power plant steam and water distribution lines, underground electrical power transmission lines, thermal insulation of pipes imbedded in walls, and burial of nuclear waste.

Most existing heat transfer calculations take into account conduction alone [1–4]. However, in many cases, the medium is permeable to fluid motion. The temperature difference between the pipe and the medium surface may cause natural convection. Consequently, the heat transfer process will consist of natural convection as well as conduction. Typically, the natural convection effects are at least as important as the conductive effects.

In spite of this fact, very little has been done to study the thermal convection associated with pipes buried in a permeable medium. Schrock *et al.* [5] and Fernandez and Schrock [6] carried out experiments and numerical calculations for a cylinder buried beneath a permeable, horizontal surface. Their work resulted in a heat transfer correlation fitting their experimental and numerical data within a standard deviation of 11.4%. The boundary conditions used in their work differ, however, from those used in this paper. Hickox [7] used a regular perturbation expansion to calculate a first-order solution for a flow field induced by a point heat source. His results, however, are of significance only for deeply buried sources. That is, the source size is much smaller than the burial depth.

In this paper a regular perturbation expansion is used to calculate the flow and temperature fields associated with a pipe buried beneath an inclined surface. Both cases of permeable and impermeable top surfaces are considered. The complicated boundary conditions are handled in an elegant manner through the use of bicylindrical coordinates [8].

The results presented here are an extension of previous work [9] where thermal convection in an eccentric annulus was considered. The case of the buried pipe can be obtained as a limiting case of the eccentric annulus by extending to infinity both the radius of the outer cylinder and the eccentricity. In this previous work [9], it was demonstrated that there exists an optimal value of eccentricity for which the total heat transfer in the annulus is minimized. Similarly, one can show here that there is an optimal burial depth for which heat losses from the pipe are minimized.

The existence of such an optimal value should be taken into consideration in the design process of pipes buried in a permeable medium. Contrary to popular belief, an increase in the burial depth may not reduce the heat losses. In fact, quite the opposite is possible. The existence of such an optimal burial depth has not been pointed out before.

2. THE MATHEMATICAL MODEL AND THE SOLUTIONS PROCEDURE

Consider a pipe of radius $\hat{r}_1$ buried at a depth $\hat{d}$ beneath the surface of a fully saturated porous medium (Fig. 1). The normal to the surface forms an angle θ with the direction of the gravity vector (g). The pipe and the surface are maintained at uniform constant temperatures $\hat{T}_1$ and $\hat{T}_2$, respectively. As a result of the temperature difference $(\hat{T}_1 - \hat{T}_2)$, fluid motion is induced in the medium. Carets denote the dimensional form of variables which will later be made nondimensional.

One can formulate the problem using bicylindrical coordinates [8]. The bicylindrical coordinates are most

NOMENCLATURE

a	scale factor for the bicylindrical coordinates, ($\sinh \alpha_1$)
d	burial depth
g	gravity vector
G, H	functions, equation (6)
k_{eq}	equivalent thermal conductivity of the porous medium
N_s	coefficient in the expansion for the Nusselt number
Nu	Nusselt number, $Q/Q_{conduction}$
Q	heat flow per unit length of the pipe, $\hat{Q}/k_{eq}(\hat{T}_1 - \hat{T}_2)$
q	heat flux, $\hat{q}r_1/k_{eq}(\hat{T}_1 - \hat{T}_2)$
R	Rayleigh–Darcy number, $\beta^* g\lambda \hat{r}_1(\hat{T}_1 - \hat{T}_2)/\alpha_{eq}\nu$
R_{eff}	effective Rayleigh–Darcy number, $R\hat{d}/\hat{r}_1$
r_1	pipe radius
T	temperature
x, y	Cartesian coordinates (Fig. 1).

Greek symbols

α, β	bicylindrical coordinates
α_{eq}	equivalent thermal diffusivity of the saturated porous medium
β^*	thermal expansion coefficient
θ	inclination angle
λ	permeability
ν	kinematic viscosity
ρ	density
ψ	stream function.

Subscripts

1	pipe surface
2	surface of the semi-infinite media.

Superscript

$\hat{}$	dimensional quantities.

natural for this problem since the physical boundaries (i.e. the pipe and the medium surfaces) can be identified with constant value coordinates. The conversion into bicylindrical coordinates is achieved through the transformation

$$x + \mathrm{i}\, y = a \coth \frac{\alpha - \mathrm{i}\beta}{2} \tag{1}$$

where constant α lines are the circles

$$(x - a\coth\alpha)^2 + y^2 = \frac{a^2}{\sinh^2 \alpha}. \tag{2}$$

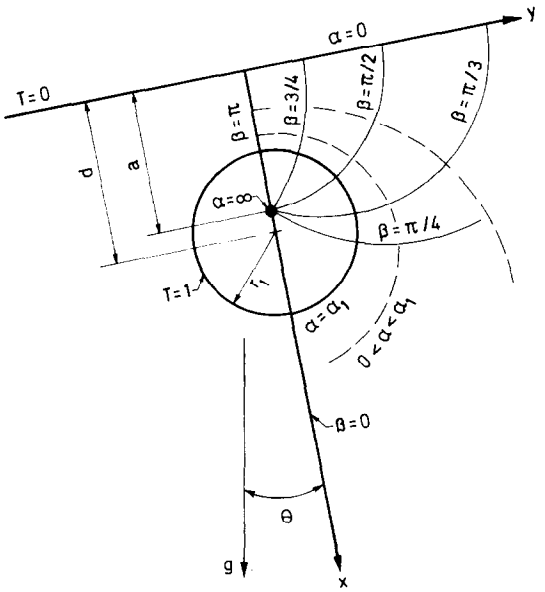

FIG. 1. The geometrical configuration and the coordinate system.

The pipe and the medium surfaces correspond to $\alpha = \alpha_1$ and 0, respectively. The burial depth $d = \cosh \alpha_1$ and the scaling $a = \sinh \alpha_1$.

The Darcy–Oberbeck–Boussinesq's equations formulated in terms of the stream function (ψ) and the temperature (T) have the form

$$\nabla^2_{\alpha\beta}\psi = aR\left\{[H(\alpha,\beta)\sin\theta + G(\alpha,\beta)\times\cos\theta]\frac{\partial T}{\partial\alpha} + [H(\alpha,\beta)\cos\theta - G(\alpha,\beta)\sin\theta]\frac{\partial T}{\partial\beta}\right\} \tag{3}$$

$$\nabla^2_{\alpha\beta}T = \frac{\partial\psi}{\partial\alpha}\frac{\partial T}{\partial\beta} - \frac{\partial\psi}{\partial\beta}\frac{\partial T}{\partial\alpha}$$

where

$$\nabla^2_{\alpha\beta} = \frac{\partial^2}{\partial\alpha^2} + \frac{\partial^2}{\partial\beta^2}$$

and the boundary conditions are

$$\psi = 0; \quad T = 1 \quad \text{at} \quad \alpha = \alpha_1 \tag{4}$$

and

$$\psi = 0; \quad T = 0 \quad \text{at} \quad \alpha = 0 \quad \text{(impermeable surface)}$$

or

$$\frac{\partial\psi}{\partial\alpha} = 0; \quad T = 0 \quad \text{at} \quad \alpha = 0 \quad \text{(permeable surface)}.$$

Additionally, one requires

$$\psi, T(\alpha, \beta + 2\pi) = \psi, T(\alpha, \beta). \tag{5}$$

The functions H and G are

$$H(\alpha,\beta) = \frac{1 - \cosh\alpha\cos\beta}{(\cosh\alpha - \cos\beta)^2}$$

and

$$G(\alpha,\beta)=\frac{\sinh\alpha\sin\beta}{(\cosh\alpha-\cos\beta)^2}. \tag{6}$$

The equations are written in a nondimensional form in which one scales the length with $\hat{r}_1$, the velocity with $\alpha_{eq}/\hat{r}_1$ and the temperature with $(\hat{T}_1-\hat{T}_2)$. The Darcy–Rayleigh number R is based on the pipe radius. The effective Rayleigh number (R_{eff}) differs from R and is equal to $R\hat{d}/\hat{r}_1 = R\cosh\alpha_1$.

Once the temperature field and the stream function are determined, the local heat flux (q) at the pipe ($\alpha=\alpha_1$) or the medium surface ($\alpha=0$) can be readily obtained

$$q=\left(\frac{\cosh\alpha-\cos\beta}{a}\frac{\partial T}{\partial\alpha}\right)_{\alpha=\alpha_1 \text{ or } 0} \tag{7}$$

The heat flow Q per unit length of pipe is

$$Q=\int_{-\pi}^{\pi}\left(\frac{\partial T}{\partial\alpha}\right)_{\alpha=\alpha_1 \text{ or } 0}\mathrm{d}\beta \tag{8}$$

and the Nusselt number (Nu) is

$$Nu=\frac{Q}{Q_{\text{conduction}}}=\frac{\alpha_1}{2\pi}Q. \tag{9}$$

One can proceed to solve the above equations by using a regular perturbation expansion in terms of the Rayleigh number (R)

$$T=\sum_{s=0}^{\infty}(aR)^sT_s;\quad \psi=\sum_{s=0}^{\infty}(aR)^s\psi_s;$$
$$\text{and}\quad Nu=\sum_{s=0}^{\infty}(aR)^sN_s. \tag{10}$$

Next, one introduces this expansion into the differential equation (3), compare the terms of the same power in s and obtain for each level of approximation a set of linear differential equations. Before proceeding to solve these equations, it is convenient to expand H and G [equation (6)] into their corresponding Fourier series. The resulting equations of order s are

$$\nabla^2_{\alpha\beta}\psi_s=2\sum_{k=1}^{\infty}k\,\mathrm{e}^{-k\alpha}\left[\frac{\partial T_{s-1}}{\partial\alpha}\sin(k\beta-\theta)-\frac{\partial T_{s-1}}{\partial\beta}\cos(k\beta-\theta)\right]$$
$$\nabla^2_{\alpha\beta}T_s=\sum_{j=1}^{s}\left(\frac{\partial\psi_j}{\partial\alpha}\frac{\partial T_{s-j}}{\partial\beta}-\frac{\partial\psi_j}{\partial\beta}\frac{\partial T_{s-j}}{\partial\alpha}\right) \tag{11}$$

and the contribution to the Nusselt number is

$$N_s=\frac{\alpha_1}{2\pi}\int_{-\pi}^{\pi}\left(\frac{\partial T_s}{\partial\alpha}\right)_{\alpha=\alpha_1 \text{ or } 0}\mathrm{d}\beta. \tag{12}$$

3. THE PERTURBATION EXPANSION

In this section analytical results for the lower order approximations are presented. The results presented, unless otherwise specified, apply to both porous media with impermeable surfaces and those with permeable surfaces. For the sake of brevity these two cases are referred to as impermeable and permeable, respectively.

3.1. *The zero-order solution* ($s=0$)

The zero-order solution corresponds to the state of pure conduction (no fluid motion). Thus

$$T_0=\frac{\alpha}{\alpha_1};\quad \psi_0=0;\quad \text{and}\quad N_0=1. \tag{13}$$

3.2. *First-order solution* ($s=1$)

For the first-order, equation (11) becomes

$$\nabla^2\psi_1=\frac{2}{\alpha_1}\sum_{k=1}^{\infty}k\,\mathrm{e}^{-k\alpha}\sin(k\beta-\theta)$$
$$\nabla^2T_1=\frac{1}{\alpha_1}\frac{\partial\psi_1}{\partial\beta} \tag{14}$$

with the appropriate boundary conditions.

Equation (14) admits a solution of the form

$$\psi_1=\sum_{n=1}^{\infty}g_{1,n}\sin(n\beta-\theta)$$
$$T_1=\sum_{n=1}^{\infty}f_{1,n}\cos(n\beta-\theta) \tag{15}$$

where for the *impermeable* case

$$g_{1,n}=\mathrm{e}^{-n\alpha_1}\frac{\sinh n\alpha}{\sinh n\alpha_1}-\frac{\alpha}{\alpha_1}\mathrm{e}^{-n\alpha}$$
$$f_{1,n}=\frac{1}{4}\mathrm{e}^{-n\alpha_1}\left\{1+\frac{1}{n\alpha_1}+2\coth(n\alpha_1)\right\}\times\frac{\sinh n\alpha}{\sinh n\alpha_1}-\frac{1}{2}\frac{\alpha}{\alpha_1}\mathrm{e}^{-n\alpha_1}\frac{\cosh n\alpha}{\sinh n\alpha_1}-\frac{\alpha}{4\alpha_1^2}\left(\alpha+\frac{1}{n}\right)\mathrm{e}^{-n\alpha},\quad 0<\alpha<\alpha_1 \tag{16}$$

and for the *permeable* case

$$g_{1,n}=-\frac{\alpha}{\alpha_1}\mathrm{e}^{-n\alpha}+\frac{\mathrm{e}^{-n\alpha_1}\cosh n\alpha}{\cosh n\alpha_1}+\frac{1}{n\alpha_1}\frac{\sinh n(\alpha-\alpha_1)}{\cosh n\alpha_1}$$
$$f_{1,n}=-\frac{\alpha}{4\alpha_1^2}\left(\alpha+\frac{1}{n}\right)\mathrm{e}^{-n\alpha}-\frac{(\alpha-\alpha_1)}{2\alpha_1\cosh n\alpha_1}\times\left[\mathrm{e}^{-n\alpha_1}\sinh n\alpha+\frac{1}{n\alpha_1}\cosh n(\alpha-\alpha_1)\right]+\frac{1}{2\sinh n\alpha_1}\left[\frac{1}{n\alpha_1}\sinh[n(\alpha-\alpha_1)]+\frac{1}{2}\left(1+\frac{1}{n\alpha_1}\right)\mathrm{e}^{-n\alpha_1}\sinh n\alpha\right],\quad 0\leqslant\alpha\leqslant\alpha_1. \tag{17}$$

One observes that some of the terms in the above expressions [equations (16) and (17)] may converge slowly. This can be cured, however, by identifying some of the infinite series with known analytical functions to

obtain

$$\psi_1 = -\frac{1}{2}\frac{\alpha}{\alpha_1}\frac{\sin(\beta-\theta)+e^{-\alpha}\sin\theta}{\cosh\alpha-\cos\beta}+\sum_{n=1}^{\infty}e^{-n\alpha_1}\times\frac{\sinh n\alpha}{\sinh n\alpha_1}\sin(n\beta-\theta)$$

$$T_1 = -\frac{1}{8}\left(\frac{\alpha}{\alpha_1}\right)^2\frac{\cos(\beta-\theta)-e^{-\alpha}\cos\theta}{\cosh\alpha-\cos\beta}-\frac{1}{4}\frac{\alpha}{\alpha_1^2}\times\left\{\cos\theta\left[\frac{\alpha}{2}-\frac{1}{2}\ln[2(\cosh\alpha-\cos\beta)]\right]\right.$$

$$\left.+\sin\theta\tan^{-1}\left(\frac{\sin\beta}{e^{\alpha}-\cos\beta}\right)\right\}-\sum_{n=1}^{\infty}\times\left\{\frac{\alpha-\alpha_1}{2\alpha_1\cosh n\alpha_1}\left[e^{-n\alpha_1}\sinh n\alpha+\frac{1}{n\alpha_1}\cosh[n(\alpha-\alpha_1)]\right]\right\}-\frac{1}{2\sinh n\alpha_1}\times\left[\frac{1}{n\alpha_1}\sinh[n(\alpha_1-\alpha)]+\frac{1}{2}\left(1+\frac{1}{n\alpha_1}\right)\times e^{-n\alpha_1}\sinh n\alpha\right]\right\}\cos(n\beta-\theta). \quad (19)$$

for the *permeable* case.

A rather peculiar property of the first-order solution is its invariance to π rotation

$$\psi_1(\alpha,\beta,\theta) = -\psi_1(\alpha,\beta,\theta+\pi) \quad (20)$$

which implies, for example, that the first-order flow fields, with the exception of the change in the direction of the flow, is exactly the same for a pipe buried beneath the surface as for a pipe located above the surface of a semi-infinite medium. This suggests that the first-order solution is valid only for very low Rayleigh numbers.

Note that in the impermeable case the value of the stream function at infinity is zero. (The infinity in the physical plane corresponds to $\alpha = \beta = 0$.) In general, however, this is not true for the permeable case where the value of the stream function grows without limit as one approaches infinity. In spite of this fact, in both cases the velocity is zero at infinity. Therefore, both solutions are physically acceptable.

Although the first-order solution modifies the local heat flux on both the cylinder's and the medium's surfaces, there is no net contribution to the total heat flow. That is

ref. [9]).

One can note that in order to obtain the second-order correction to the Nusselt number (N_2) no knowledge of the second-order solution is required since

$$N_2 = (\alpha_1-\alpha_2)\left.\frac{df^1_{2,0}}{d\alpha}\right|_{\alpha=\alpha_1 \text{ or } 0} = \frac{1}{2}\sum_{i=1}^{\infty} i\int_{\alpha_1}^{0} f_{1,i}g_{1,i}\,d\alpha. \quad (23)$$

Calculated values of a^2N_2 are presented in Fig. 2 for both the impermeable and permeable cases and for the burial depths: $1 < d/r_1 < 14$.

The second-order correction to the Nusselt number is independent of the inclination angle θ. Note that the second-order correction to the Nusselt number has been constructed from the first-order solution. Therefore, this is not a complete surprise in view of the first-order solution's invariance to π rotation. This independence of θ suggests that the first-order solution may be valid only for very low Rayleigh numbers. In order to investigate the effect of the inclination (θ) on the heat transfer one is forced to proceed to the next level of approximation.

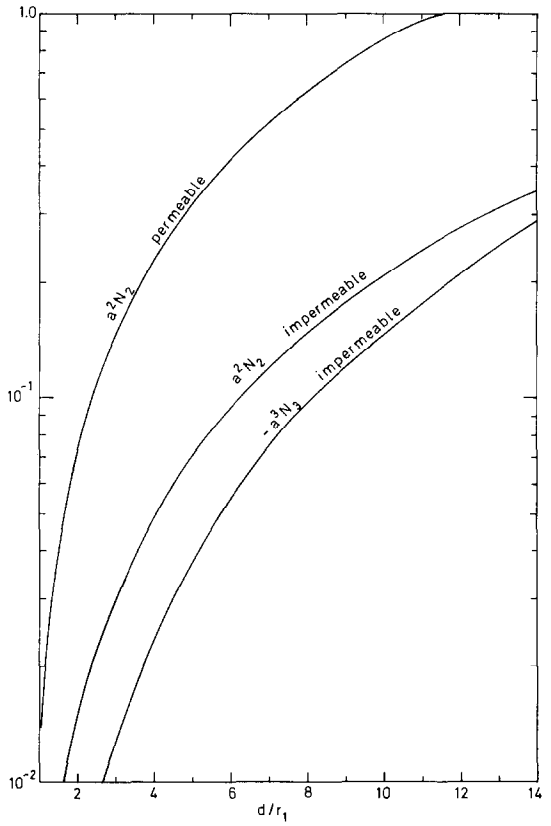

FIG. 2. The first-order correction for the Nusselt number (a^2N_2) for both the impermeable and the permeable cases, and the second-order correction a^3N_3 for the permeable case only.

3.4. *Third-order solution* ($s = 3$)

The algebra involved in constructing this order of solution is even more tedious than the second-order solution. Here the goal is merely to assess the effect of the inclination angle (θ) on the Nusselt number. As in the previous section, the correction to the Nusselt number is constructed from the lower-order solution and fortunately detailed knowledge of the third-order solution is not needed. One finds that

$$N_3 \cos\theta = \frac{1}{2}\cos\theta \sum_{i=1}^{\infty} i \int_{\alpha_1}^{0} [f_{1,i}(g^{\mathrm{I}}_{2,i}+g^{\mathrm{II}}_{2,i}) + g_{1,i}(f^{\mathrm{I}}_{2,i}+f^{\mathrm{II}}_{2,i})]\,\mathrm{d}\alpha. \quad (24)$$

That is the third-order term has $\cos\theta$ dependence. The calculation of N_3 involves slowly converging series, thus we carried out the calculation only for the impermeable case. The results are depicted in Fig. 2.

4. RESULTS AND DISCUSSION

4.1. *The flow and temperature fields*

The flow and temperature fields are depicted in Figs. 3–9 for pipes buried in semi-infinite media with impermeable and permeable surfaces, and with inclination angles $\theta = 0$, $\pi/4$ and $\pi/2$.

The flow and temperature fields associated with pipes buried beneath impermeable and permeable horizontal surfaces ($\theta = 0$) are shown in Figs. 3 and 4. The streamlines and the isotherms are shown on the RHS and LHS of the figures, respectively. The streamlines correspond to the first-order solution (ψ_1); and the increment between any two neighboring streamlines is uniform.

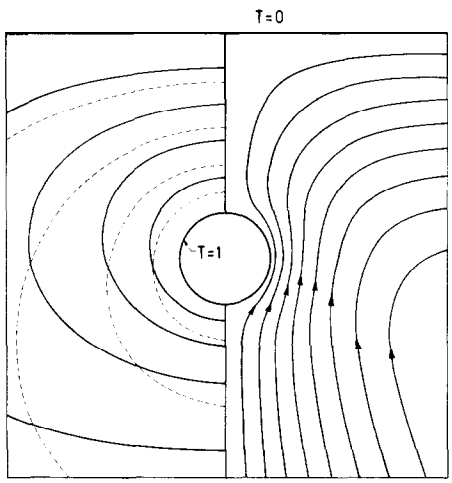

FIG. 3. The uniformly spaced streamlines (ψ_1) and the isotherms ($T_0 + aRT_1$) are shown on the RHS and LHS of the figure, respectively. The solid and dashed lines correspond to the temperature fields at $R = 2(R_{\mathrm{eff}} = 10)$ and 0, respectively. The top surface is horizontal ($\theta = 0$) and impermeable.

The solid lines on the LHS of Figs. 3 and 4 represent the isotherms ($T_0 + aRT_1$) corresponding to $R = 2(R_{\mathrm{eff}} = 10)$ while the dashed lines depict the isotherms in the absence of motion ($R = 0$). The increment between neighboring isotherms is 0.2. The distortion of the temperature field as a result of the motion is self-evident.

The results in Fig. 4 are in good qualitative agreement with the finite-difference calculations exhibited in ref. [6] and with the flow field associated

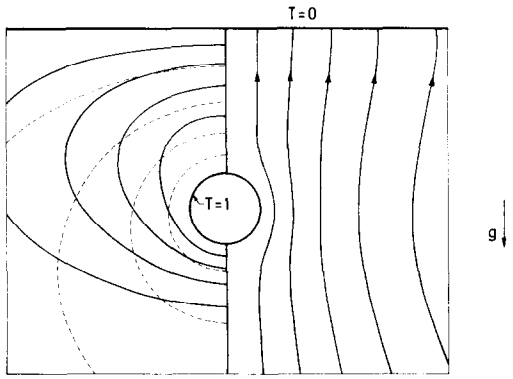

FIG. 4. Uniformly spaced streamlines (ψ_1) and isotherms ($T_0 + aRT_1$) are shown on the RHS and LHS of the figure, respectively. The solid dashed lines correspond to the temperature fields at $R = 2(R_{\mathrm{eff}} = 10)$ and 0, respectively. The top surface is horizontal ($\theta = 0$) and permeable.

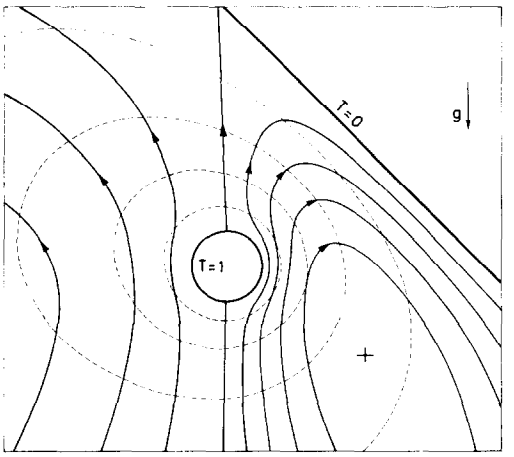

FIG. 5. The solid and dashed lines represent uniformly spaced streamlines (ψ_1) and isotherms ($T_0 + aRT_1$). The surface of the medium is impermeable and inclined at $\theta = \pi/4$. The (+) denotes the location of $|\psi_{max}|$. The temperature field corresponds to $R = 1$ ($R_{eff} = 5$).

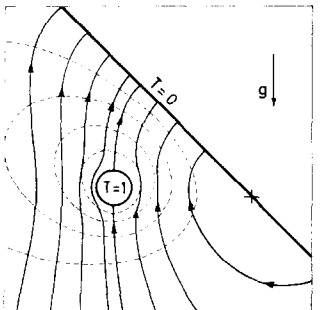

FIG. 6. The solid and dashed lines represent uniformly spaced streamlines (ψ_1) and isotherms ($T_0 + aRT_1$). The surface of the medium is permeable and inclined at $\theta = \pi/4$. The (+) denotes the location of $|\psi_{max}|$. The temperature field corresponds to $R = 1$ ($R_{eff} = 5$).

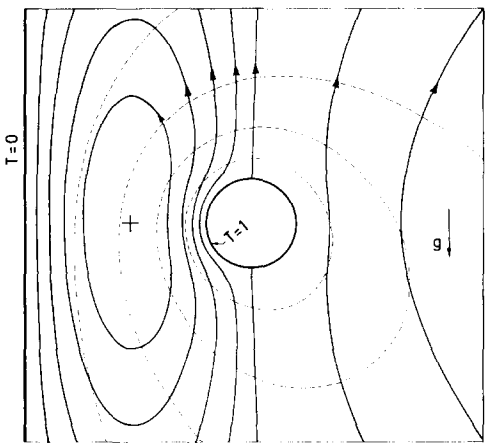

FIG. 7. The solid and dashed lines represent uniformly spaced streamlines (ψ_1) and isotherms ($T_0 + aRT_1$). The surface of the medium is impermeable and inclined at $\theta = \pi/2$ (vertical). The (+) denotes the location of $|\psi_{max}|$. The temperature field corresponds to $R = 1$ ($R_{eff} = 5$).

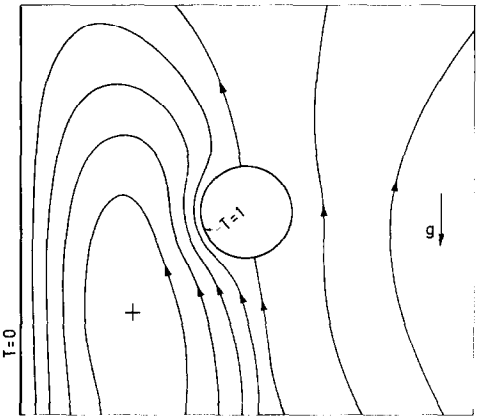

FIG. 8. Uniformly spaced streamlines are shown for the second-order solution $aR(\psi_1 + aR\psi_2)$. The flow field corresponds to $R = 2$ ($R_{eff} = 10$). The medium surface is impermeable and inclined at $\theta = \pi/2$ (vertical). The (+) denotes the location of $|\psi_{max}|$.

with a sphere buried beneath a permeable surface as presented in ref. [7].

In the case of the horizontal surface ($\theta = 0$), the flow and temperature fields are symmetric with respect to the vertical axis (x in Fig. 1). In the impermeable case, the streamlines consist of closed curves; while in the permeable case, the streamlines do not close inside the porous medium. In the latter case fluid is fed into the porous medium far away from the location of the pipe (not shown in Fig. 4).

By comparing Figs. 3 and 4 one can note that in the latter the distortion of the temperature field is more profound. This difference can be ascribed to the more intense circulation in the permeable case. For example, $|\psi_{max}|$ in Fig. 4 is about twice as large as $|\psi_{max}|$ in Fig. 3. A similar trend is exhibited in the Nusselt number correlation (Fig. 2).

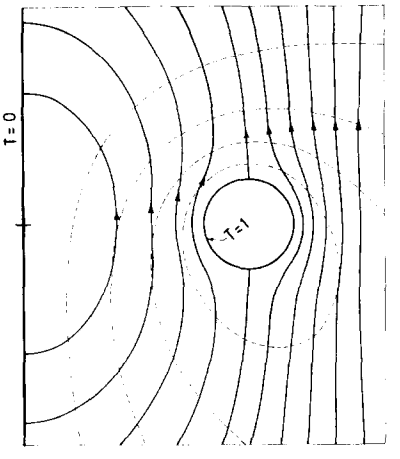

FIG. 9. The solid and dashed lines represent uniformly spaced streamlines (ψ_1) and isotherms ($T_0 + aRT_1$). The surface of the medium is permeable and inclined at $\theta = \pi/2$ (vertical). The (+) denotes the location of $|\psi_{max}|$. The temperature field corresponds to $R = 1$ ($R_{eff} = 5$).

It has already been noted that the first-order solution (ψ_1) is invariant to π rotation. Consequently by inverting the figures and the arrows on the streamlines, one can obtain the first-order flow field for the case of a surface beneath the pipe.

Next one proceeds to study the effect of the angle of inclination (θ) on the flow and temperature fields. In Figs. 5 and 6 the solid and dashed lines depict the first-order solutions for the stream-function (ψ_1) and the isotherms ($T_0 + aRT_1$), respectively. Figures 5 and 6 correspond to the impermeable and permeable cases, respectively. The increments between both neighboring streamlines and neighboring isotherms are uniform. The temperature field corresponds to $R = 1$ ($R_{\text{eff}} = 5$). Clearly, the symmetry observed in the horizontal case ($\theta = 0$) disappears here as the flow aligns itself in the gravity field.

Due to the invariance of the flow field (ψ_1) to π rotation, one can obtain from Figs. 5 and 6 the flow field associated with $\theta = 5\pi/4$ and $3\pi/4$ (the pipe is above the surface). The former is obtained by π rotation of Figs. 5 and 6 and the latter by mirror reflection of the flow field associated with $\theta = 5\pi/4$. Note that the above does not hold for the temperature field depicted in Figs. 5 and 6.

Finally, in Figs. 7 and 9, the case of a vertical boundary ($\theta = \pi/2$) is depicted for the impermeable and permeable surfaces, respectively. The streamlines (ψ_1) and the isotherms ($T_0 + aRT_1$) are plotted in solid and dashed lines.

The flow field is symmetric with respect to the horizontal axis (x in Fig. 1). The center of rotation (the location of $|\psi_{\max}|$, $(+)$) is located on the same axis. This is, of course, in accord with the invariance of the first-order solution (ψ_1) to π rotation. However, it is somewhat in contrast with the physical intuition, since one expects the flow to be skewed towards the vertical boundary. In order to investigate this point in somewhat more detail the two-term expansion was calculated $aR(\psi_1 + aR\psi_2)$. One finds that the flow field depicted in Fig. 7 is valid only for very low Rayleigh numbers (i.e. the flow field in Fig. 7 corresponds to $R < 0.2$, $R_{\text{eff}} < 1$). The flow field associated with higher Rayleigh numbers is depicted in Fig. 8 ($R = 2$). Clearly, the symmetry observed in Fig. 7 with respect to the horizontal axis no longer exists. The dividing streamline ($\psi = 0$) is now inclined towards the wall, as indeed, should be the case.

4.2. *Heat transfer*

In Section 3 the following expression for the Nusselt number was obtained

$$Nu = 1 + a^2N_2R^2 + a^3N_3R^3\cos\theta + \cdots \qquad (25)$$

Values of a^2N_2 for both the permeable and impermeable surfaces as well as values of a^3N_3 for the impermeable case are depicted in Fig. 2. One can note in passing that the values of a^2N_2 for the permeable case are markedly higher than those for the impermeable case. This is apparently a result of the more intense circulation observed in the former case as is evident from Figs. 3 and 4.

In what follows, the behavior of series (25) for the impermeable case only is investigated. Series (25) is a slowly converging one. For example, for a burial depth $d = 5$ one obtains $a^2N_2 = 0.07$ and $a^3N_3 = 0.037$. Clearly, meaningful results can be obtained only for relatively small values of R. Comparison with a finite-difference numerical simulation for $\theta = 0$ and π shows that one has a good agreement only for $R_{\text{eff}} < 5$ ($R < 1$). Similar results are obtained for other burial depths as well.

The range of utility of series (25) for the Nusselt number is quite disappointing. In an attempt to improve the performance of series (25) Shank's transformation [10] is used to obtain

$$Nu = 1 + \frac{(a^2N_2R)^2}{a^2N_2 - a^3N_3R\cos\theta}. \qquad (26)$$

The values of a^2N_2 and a^3N_3 are given in Fig. 2. Alternatively, for $2 \leqslant d \leqslant 14$, they may be calculated using the following formulas

$$a^2N_2 = 10^{-3}(-10.12 + 9.335d + 1.523d^2 - 0.034d^3)$$

$$a^3N_3 = 10^{-3}(1.599 - 1.865d^2 + 0.148d^3 - 0.005d^4).$$

In order to estimate the range of validity of correlation (26) for $\theta = 0$, a finite-difference numerical simulation is used. To this end, the nonlinear equations (3) are solved using Patankar's power law technique [11]. The number of grid points is typically about 500. The resulting difference equations are solved by successive over-relaxation (SOR). The convergence criteria requires that the maximum relative variation of the local stream function and the temperature be smaller than a prescribed value (10^{-3}). The heat flow at both the pipe and the medium surfaces is also calculated. The deviation is typically well below 0.2%.

In Fig. 10, the Nusselt number predicted by equation (26) is depicted as a function of the Rayleigh number (R), for various burial depths and for $\theta = 0$. These results, equation (26) (solid lines), are compared in Fig. 10 with those of the numerical simulation (symbols). For $R_{\text{eff}} = Rd/r_1 < 60$, the deviation between the analytical, equation (26), and the numerical results is well below 5%. This is, indeed, an exciting result. Through the use of the nonlinear transformation, equation (26), one can extend the usefulness of the three-term series (26) from a meager $R_{\text{eff}} \sim 5$ to a respectable $R_{\text{eff}} \sim 60$.

In the above equation (26) was used solely in the case of $\theta = 0$ (a pipe buried beneath a horizontal, impermeable surface). Equation (26) is expected to extend the range of validity of equation (25) for $0 \leqslant \theta < \pi/2$. For $\theta = \pi/2$, equation (25) is recovered from equation (26). For $\theta > \pi/2$, equation (26) has a singularity at $R = a^2N_2/a^3N_3 \cos\theta$ (recall: $a^3N_3 < 0$), which may affect adversely its range of validity. For $\theta = \pi$, one finds that equation (26) is doing as badly as equation (25). Therefore, one can conclude that expression (26) is probably useful only for $0 \leqslant \theta \leqslant \pi/2$.

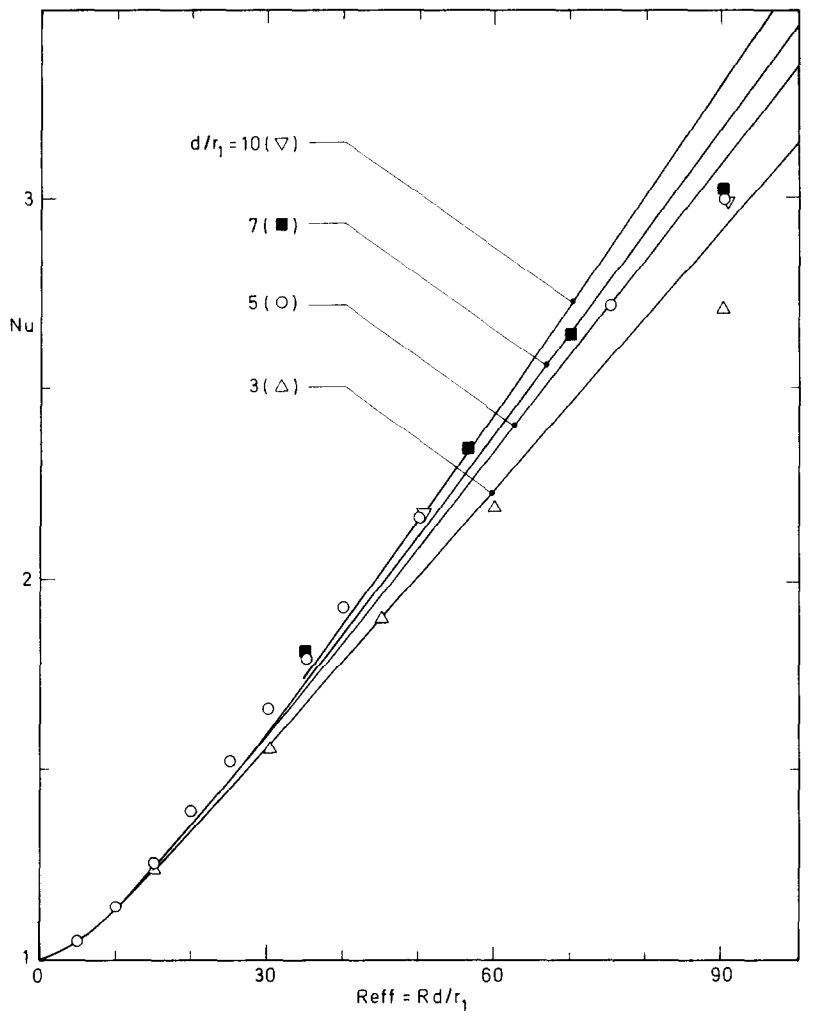

FIG. 10. The Nusselt number predicted by equation (26) (solid line) is compared with results of a finite-difference numerical simulation (symbols) for various burial depths $\hat{d}/\hat{r}_1 = 3, 5, 7$, and 10.

A more thorough examination of the range of validity of the transformed expression (26), for $\theta \neq 0$, requires numerous numerical experiments. In this paper, one focuses, however, on an analytical derivation; therefore, such an investigation will be deferred to another occasion.

Next, correlation (26) is used to investigate the effect of the burial depth on the heat transfer from the pipe to the medium surface. The heat flow per unit length of the pipe ($Q/2\pi = Nu/\alpha_1$) as a function of the burial depth ($\hat{d}/\hat{r}_1$) is depicted in Fig. 11 (solid lines) for Rayleigh numbers, $R = 0, 2, 3.5, 5$ and 10. For $R = 5$ and 10, we also present results of the numerical simulation (circles). Clearly, there is fairly good agreement between the analytical (solid lines) and the numerical (circles) predictions. For $R > 0$, the heat losses initially decrease with increasing burial depth, reach a minimum and then increase again. That is, there is an optimal depth for which the heat losses are minimized. The value of the optimal depth is a function of the Rayleigh number. The magnitude of the optimal burial depth decreases as the Rayleigh number (R) increases. This trend is described schematically by the dashed line in Fig. 11.

The physical explanation for this phenomena is rather simple. Recall that the heat transfer process consists of both conduction and natural convection. As the burial depth increases, the conductive heat losses are reduced as shown by the curve $R = 0$ in Fig. 11. At the same time, however, the effective Rayleigh number ($R_{\text{eff}} = R\hat{d}/\hat{r}_1$) increases, which implies, for the burial depths considered, a more intense circulation and higher losses by convection. Consequently, there is some optimal value for which the total heat transfer is minimized. As the Rayleigh number (R) increases, the convection plays a more important role and therefore the magnitude of the optimal value decreases.

Finally, for demonstration purposes, the magnitude of heat losses and potential energy savings are examined in the case of a pipe of radius $\hat{r}_1 = 0.25$ m buried beneath an isothermal and impermeable surface. Suppose the soil outside the pipe is silica sand (average grain size of about 2.54×10^{-4} m) and

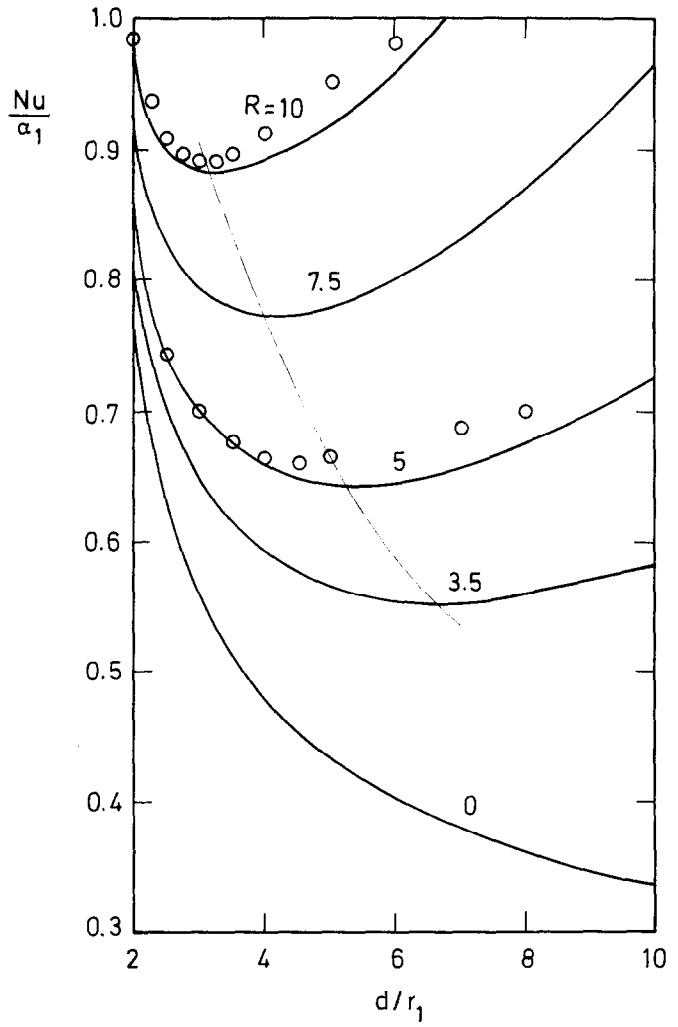

FIG. 11. The heat losses (Nu/α_1) as functions of the burial depth for various Rayleigh numbers, $R = 0, 2, 3.5, 5$, and 10. The solid lines represent the analytical solution while the circles are a result of numerical simulations.

permeability $\lambda \sim 6 \times 10^{-11}$ m^2. The temperature difference between the pipe and the earth's surface is $\hat{T}_1 - \hat{T}_2 = 60°C$. The saturating fluid is water and its properties are evaluated at 40°C. The corresponding Darcy–Rayleigh number is $R \sim 10$. For a pipe buried at the depth $d = 2$ m ($\hat{d}/\hat{r}_1 = 8$), $Nu = 2.8$. Thus, the thermal convection represents two-thirds of the total heat losses. If the pipe were buried at a depth $\hat{d} = 0.9$ m ($\hat{d}/\hat{r}_1 = 3.5$), energy savings of about 13% would be realized.

5. CONCLUSION

A regular perturbation expansion has been used to solve for the flow and temperature fields around a pipe buried in a permeable medium. Analytical expressions are obtained for the stream function and the temperature. The expressions, although formally valid only for small Rayleigh numbers ($R < 1$), probably provide a good qualitative description of the flow for larger values of the Rayleigh number as well. A correlation in the form of a power series in terms of the Rayleigh number is obtained for the Nusselt number. The range of validity of the series is very small. However, the use of a nonlinear transformation enables one to increase considerably the range of utility of the series. Finally, one demonstrates that there exists an optimal burial depth for which the heat transport from the pipe is minimized. The fact that there exists an optimal burial depth should be taken into consideration while designing pipelines since one may achieve considerable energy savings by selecting the correct burial depth.

Acknowledgement—This material is based upon work supported, in part, by the National Science Foundation, under Grant No. MEA 8217565.

REFERENCES

1. E. R. G. Eckert and R. M. Drake, *Analysis of Heat and Mass Transfer*, pp. 92–102. McGraw-Hill, New York (1972).
2. N. N. Lebedev, I. P. Skalakaya and Y. S. Uflyand, *Worked*

Problems in Applied Mathematics, pp. 242–247. Dover, New York (1979).
3. H. H. Bau and S. S. Sadhal, Heat losses from a fluid flowing in a buried pipe, *Int. J. Heat Mass Transfer* **25,** 1621–1629 (1982).
4. R. F. DiFelice and H. H. Bau, Conductive heat transfer between eccentric cylinders with boundary conditions of the third kind, *Trans. Am. Soc. Mech. Engrs*, Series C, *J. Heat Transfer* **105,** 678–680 (1983).
5. V. E. Schrock, R. T. Fernandez and K. Kesavan, Heat transfer from cylinders embedded in a liquid filled porous medium, *Proc. Int. Heat Transfer Conf.*, Paris, Vol. VII, CT 3.6 (1970).
6. R. T. Fernandez and V. E. Schrock, Natural convection from cylinders buried in a liquid-saturated porous medium, *Proc. Int. Heat Transfer Conf.*, Munich, Vol. 2, pp. 335–340 (1982).
7. C. E. Hickox, Thermal convection at low Rayleigh number from concentrated sources in porous media, *Trans. Am. Soc. Mech. Engrs*, Series C, *J. Heat Transfer* **103,** 232–236 (1981).
8. P. Moon and D. E. Spencer, *Field Theory Handbook*, pp. 64, 89. Springer, New York (1971).
9. H. H. Bau, Buoyancy induced flow in porous medium bounded by two eccentric cylinders, *Trans. Am. Soc. Mech. Engrs*, Series C, *J. Heat Transfer* **106,** 166–175 (1984).
10. D. Shanks, Non-linear transformations of divergent and slowly convergent sequences, *J. Math. Phys.* **34,** 1–42 (1955).
11. S. V. Patankar, *Numerical Heat Transfer and Fluid Flow*. McGraw-Hill, New York (1982).

PERTE DE CHALEUR CONVECTIVE D'UN TUBE NOYE DANS UN MILIEU POREUX SEMI-INFINI

Résumé—On présente une solution analytique pour la convection permanente à faible nombre de Rayleigh induite par un tube noyé dans un milieu saturé, perméable et semi-infini. La surface du milieu peut être inclinée par rapport au vecteur pesanteur. Les surfaces du cylindre et du milieu sont maintenues à des températures uniformes et constantes. On considère deux cas. Dans le premier, la surface du milieu est imperméable au mouvement du fluide tandis que dans l'autre la percolation à travers cette surface est possible. La géométrie compliquée est traitée d'une façon élégante en utilisant des coordonnées bicylindriques. Les résultats incluent une description des champs de vitesse et de température, aussi bien qu'une expression du nombre de Nusselt. De plus, on montre qu'il existe une profondeur optimale d'enfouissement pour laquelle les pertes thermiques du tube sont minimisées. Les résultats analytiques sont comparés avec des calculs numériques.

KONVEKTIVE WÄRMEVERLUSTE VON EINEM ROHR, DAS IN EINEM HALBUNENDLICHEN PORÖSEN MEDIUM EINGEGRABEN IST

Zusammenfassung—Eine analytische Lösung für die stationäre Konvektionsströmung bei kleinen Rayleigh-Zahlen wird vorgestellt, welche an einem in gesättigtem, halbunendlichem, permeablem Medium befindlichen Rohr zustandekommt. Die Oberfläche des Mediums darf gegenüber dem Schwerkraftvektor geneigt sein. Sowohl die Zylinder- als auch die Oberfläche des Mediums werden auf konstanter, gleichmäßiger Temperatur gehalten. Zwei Fälle werden betrachtet. Im ersten Fall ist die Oberfläche des Mediums bezüglich der Flüssigkeitsbewegung undurchlässig, während im enderen Fall Flüssigkeit durch diese Oberfläche hindurchsickern darf. Die komplizierte Geometrie wird auf elegante Weise durch die Benutzung von bizylindrischen Koordinaten erfaßt. Die Ergebnisse beinhalten eine Beschreibung der Strömungs- und der Temperaturfelder und eine Beziehung für die Nusselt-Zahl. Zusätzlich wird noch gezeigt, daß eine optimale Eingrabtiefe besteht, für welche die Wärmeverluste des Rohres minimiert werden können. Die analytischen Ergebnisse werden mit numerischen Berechnungen verglichen.

КОНВЕКТИВНЫЙ ТЕПЛООБМЕН ЗАГЛУБЛЕННОЙ ТРУБЫ С ПОЛУБЕСКОНЕЧНОЙ ПОРИСТОЙ СРЕДОЙ

Аннотация—Представлено аналитическое решение для стационарной конвекции, вызванной трубой, помещенной в насыщенную полуограниченную, проницаемую среду. Рассмотрен случай малых чисел Рэлея. Поверхность среды может иметь наклон по отношению к направлению гравитационного поля. Как цилиндр, так и поверхность среды имеют постоянную однородную температуру. Рассматривается два случая. В первом случае поверхность среды непроницаема для жидкости, а во втором жидкость может проходить через поверхность. Корректно описывается сложная геометрия с помощью бицилиндрических координат. Получены результаты по распределениям скорости и температуры и выведено соотношение для числа Нуссельта. Кроме того, показано, что существует оптимальная глубина погружения, при которой тепловые потери трубы сводятся к минимуму. Аналитические результаты сравниваются с численными расчетами.